

# H<sub>2</sub>S Dosimetry by CuO: Towards Stable Sensors by Unravelling the Underlying Solid-State Chemistry

Sebastian Werner,<sup>[a]</sup> Clarissa Glaser,<sup>[a]</sup> Thomas Kasper,<sup>[a]</sup> Trung Nghia Nguyễn Lê,<sup>[a, c]</sup> Silvia Gross,<sup>[c]</sup> and Bernd M. Smarsly\*<sup>[a, b]</sup>

**Abstract:** The precise detection of the toxic gas H<sub>2</sub>S requires reliable sensitivity and specificity of sensors even at minute concentrations of as low as 10 ppm, the value corresponding to typical exposure limits. CuO can be used for H<sub>2</sub>S dosimetry, based on the formation of conductive CuS and the concomitant significant increase in conductance. In theory, at elevated temperature the reaction is reversed and CuO is formed, ideally enabling repeated and long-term use of one sensor. Yet, the performance of CuO tends to drop upon cycling. Utilizing defined CuO nanorods we thoroughly elucidated the associated detrimental chemical changes

directly on the sensors, by Raman and electron microscopy analysis of each step during sensing (CuO→CuS) and regeneration (CuS→CuO) cycles. We find the decrease in the sensing performance is mainly caused by the irreversible formation of CuSO<sub>4</sub> during regeneration. The findings allowed us to develop strategies to reduce CuSO<sub>4</sub> formation and thus to substantially maintain the sensing stability even for repeated cycles. We achieved CuO-based dosimeters possessing a response time of a few minutes only, even for 10 ppm H<sub>2</sub>S, and prolonged life-time.

## Introduction

Hydrogen sulfide (H<sub>2</sub>S) is a colourless, highly toxic and corrosive gas which is present in diverse chemical processes, as unwanted by-product in the production of biogas and in natural gas sources. It can lead to damages on metal surfaces, poisoning of catalysts and sensor surfaces.<sup>[1]</sup> Also, it can be lethal at quite low concentrations (500 ppm within 30–60 minutes) and causes harm at even lower concentration.<sup>[2]</sup> Since biogas and the involved anaerobic digestion of biomasses gains increasing importance as sustainable and renewable energy source, the number of biogas facilities grows accord-


ingly, and consequently corrosion and intoxication with H<sub>2</sub>S is a concern of growing significance.<sup>[3]</sup> In the light of the marked toxicity of H<sub>2</sub>S, in many countries the maximum tolerable occupational exposure limit lies at 5 ppm (Germany, USA) or 10 ppm (UK), which is quite low on an absolute scale and, as a severe requirement for a sensor, needs permanent monitoring. In the latter regard, the strong corrosive nature of H<sub>2</sub>S represents a particular challenge for sensors being permanently exposed to H<sub>2</sub>S, even at small concentrations.<sup>[4]</sup> Therefore, a practical sensor should possess a long lifetime, ideally on the order of months, for a reliable monitoring of quite small H<sub>2</sub>S concentrations at any instant. The stability of the detection signal under prolonged harsh conditions is therefore strongly determined by the detection principle and, in turn, the chemical compounds involved, which may suffer from corrosion and transformation.


Hence, there are three key properties which determine the quality of a gas sensor and still represent challenges in designing gas-sensing materials: the sensitivity, the selectivity as well as the signal and chemical stability.<sup>[5]</sup> Currently, chemiresistors and electrochemical cells (ECs) are frequently used for H<sub>2</sub>S detection and in a variety of other sensing applications (see ref. for an overview).<sup>[6]</sup> Chemiresistors, based on metal oxides such as SnO<sub>2</sub>, WO<sub>3</sub> or ZnO exhibit a certain shortcoming, as these metal oxides may interact similarly with other reductive gases, which lowers the selectivity towards H<sub>2</sub>S.<sup>[7]</sup> Additionally, CuO can be used as chemiresistor in H<sub>2</sub>S sensing, showing a high sensitivity and an improved selectivity, due to a special adsorption behaviour of H<sub>2</sub>S on CuO.<sup>[8]</sup> Moreover, sol-gel derived CuO films can be used in novel sensing methods like surface acoustic wave sensing of H<sub>2</sub>S, resulting in a better sensing performance at high relative humidity.<sup>[9]</sup> Another strategy to combine high selectivity with

[a] S. Werner, C. Glaser, T. Kasper, T. N. N. Lê, Prof. Dr. B. M. Smarsly  
Institute of Physical Chemistry  
Justus-Liebig University Giessen  
Heinrich-Buff-Ring 17, 35392 Giessen (Germany)  
E-mail: bernd.smarsly@phys.chemie.uni-giessen.de

[b] Prof. Dr. B. M. Smarsly  
Center for Materials Research  
Justus-Liebig University Giessen  
Heinrich-Buff-Ring 17, 35392 Giessen (Germany)

[c] T. N. N. Lê, Prof. Dr. S. Gross  
Dipartimento di Scienze Chimiche  
Università degli Studi di Padova  
Via Marzolo 1, 35131 Padova  
and  
INSTM, UdR di Padova  
(Italy)

 Supporting information for this article is available on the WWW under <https://doi.org/10.1002/chem.202103437>

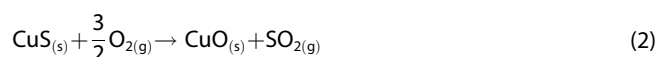
 © 2021 The Authors. Chemistry - A European Journal published by Wiley-VCH GmbH. This is an open access article under the terms of the Creative Commons Attribution Non-Commercial License, which permits use, distribution and reproduction in any medium, provided the original work is properly cited and is not used for commercial purposes.

high sensitivity is the usage of composite materials, for example doping with other metal oxides or carbon, but achieving selectivity still represents a challenge.<sup>[10]</sup> Another feasible strategy for improving H<sub>2</sub>S sensing is the concept of gas dosimetry.<sup>[11]</sup> Such sensors generally work in accumulation mode, i.e. the sensitive material reacts in a specific chemical reaction with the gas resulting in changes of electrical properties, which themselves depend on the accumulation level of the analyte. Hence, gas dosimeters measure the time to reach a defined conversion state exceeding a certain percolation threshold, at which the conductance increases steeply, i.e. if the required gas dose is reached. Based on the elapsed time span, the mean gas concentration can be calculated.<sup>[12]</sup>

The exergonic reaction of CuO with H<sub>2</sub>S forming CuS is such a reaction enabling a strategy for dosimeter-type H<sub>2</sub>S detection:



Compared to CuO, CuS has a few orders of magnitude higher charge carrier concentration. Next to CuS also Cu<sub>2</sub>S is possibly formed, which contributes to the detection of H<sub>2</sub>S, as Cu<sub>2</sub>S possesses a markedly higher conductance than CuO, too. Hence, after continuous exposure to H<sub>2</sub>S, a percolation threshold of conductive pathways of copper sulfides is exceeded, resulting in a steep, sudden decrease in resistance as macroscopic parameter. If performed below 200 °C, this reaction is both sufficiently exergonic to be thermodynamically favourable and fast enough to reach the percolation threshold within a feasible time on the order of minutes, as described recently.<sup>[13]</sup> The elapsed time until this decrease takes place is used as sensor signal and can be correlated to the concentration of H<sub>2</sub>S in the gas. As a main advantage of CuO-based H<sub>2</sub>S sensing, reaction (1) can be reversed at elevated temperature according to the principle of Le Chatelier, allowing for repeated usage of the same sensor.<sup>[14]</sup> Also, the following reaction is used in the regeneration step:



The principle of H<sub>2</sub>S detection and regeneration of such sensors is illustrated in Figure 1. One of the challenges of CuO-based H<sub>2</sub>S sensors is the stability in two important parameters of such dosimeter-type H<sub>2</sub>S sensors, upon repeated sensing (CuS formation) and regeneration (heating to transform CuS/Cu<sub>2</sub>S to CuO), namely the response time  $t_{\text{Res}}$  and the regeneration resistance  $R_{\text{Reg}}$ . The response time  $t_{\text{Res}}$  (Figure 1, turquoise bar) is the time until the decrease in resistance takes place and represents the main sensing parameter, as it varies depending on the H<sub>2</sub>S concentration.  $t_{\text{Res}}$  so far takes several minutes using CuO-based dosimetry for the detection of relevant concentrations (5 ppm, 10 ppm).<sup>[15]</sup> Further relevant parameters, which can be potentially varied, are the detection time period  $t_{\text{Detect}}$  and the regeneration time  $t_{\text{Reg}}$  (see Figure 1, and see chapter 2.3). Ideally, the resistance of copper oxide (high resistance) and that of copper sulfides (low resistance) should remain constant even after multiple cycling, or at least their relative difference. In spite of the elegance of this detection principle, in particular the stability of the sensor still impedes practical use. It is assumed that the drastic change in specific molar volume upon the transformation between CuO and CuS (and also possibly Cu<sub>2</sub>S) causes alterations in the (nano)structure and therefore results in a continuous decay in sensing performance, i.e. by a steady, irreversible increase in the resistance of the CuS material.<sup>[16]</sup> A recently introduced concept is the confinement of CuO within nanoporous scaffolds, i.e. mesoporous SiO<sub>2</sub>, in order to prevent structural rearrangement and also to achieve a faster detection owing to a large surface area. For instance, Paul et al. demonstrated that ordered mesoporous CuO/KIT-6 silica composite materials can be used for prolonged H<sub>2</sub>S sensing.<sup>[17]</sup> In a similar approach we used CuO/SiO<sub>2</sub> composites nanofibers showing a stable cycling behaviour in more than 100 sensing and regeneration cycles.<sup>[13]</sup> However, the preparation of such

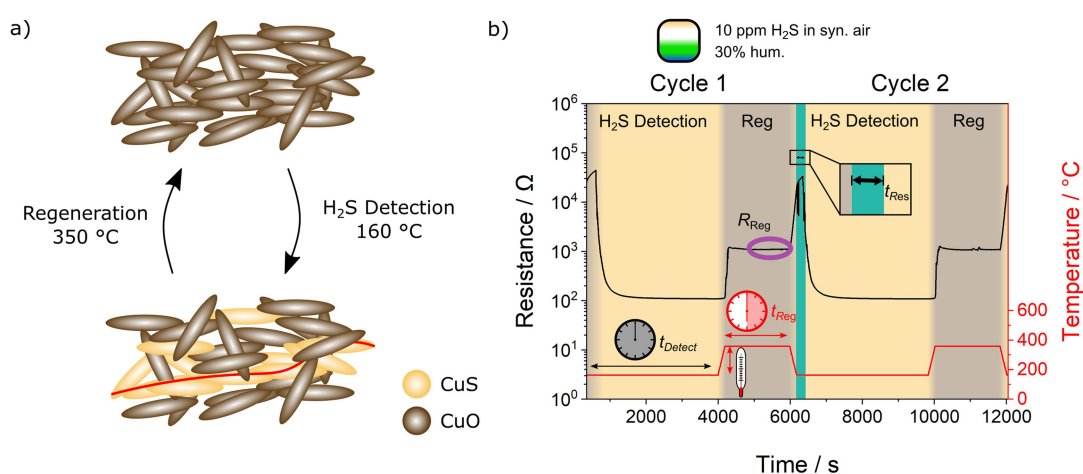
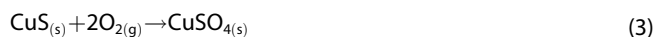


**Figure 1.** a) Schematic presentation of a sensor cycle during H<sub>2</sub>S sensing with CuO nanorods and b) the associated resistance behaviour with specific sensor settings (detection time  $t_{\text{Detect}}$ : black clock; regeneration time  $t_{\text{Reg}}$ : red clock; regeneration temperature: thermometer) and sensing parameters (regeneration resistance  $R_{\text{Reg}}$  violet circle and response time  $t_{\text{Res}}$  turquoise bar).

composites is complex, and furthermore the sensing performance decreases after a certain number of cycles.

Our recent study suggested the deterioration of the sensing performance might be caused by the formation and continuous accumulation of undesired  $\text{CuSO}_4$ .<sup>[13]</sup>

The inevitable regeneration step can involve oxidation by oxygen and thus might spur the formation of  $\text{CuSO}_4$  through the oxidation of  $\text{CuS}$  and  $\text{Cu}_2\text{S}$ :



As this reaction is highly exergonic ( $\Delta_r G^\circ \approx -608 \text{ kJ/mol}$ ),  $\text{CuSO}_4$  cannot be converted into  $\text{CuO}$  (or  $\text{Cu}_2\text{O}$ ) by means of practical regeneration conditions. For instance, the standard free enthalpy of the reaction



has a value of  $\Delta_r G^\circ \approx +180 \text{ kJ/mol}$  at  $25^\circ\text{C}$ . Based on the Gibbs-Helmholtz equation and assuming, to a first approximation,  $\Delta_r S^\circ$  and  $\Delta_r H^\circ$  being temperature-independent, a temperature of ca.  $2240 \text{ K}$  is needed to reverse equation (3) from a thermodynamic point of view, which is practically unfeasible. Thus, the almost complete irreversibility of the  $\text{CuSO}_4$  formation is inevitably a fundamental dilemma and may cause a decay in the sensing performance after a certain number of detection/regeneration steps. A practical  $\text{CuO}$ -based dosimeter-type sensor should be reliably operable without the need of replacement over a possibly long exposure time to  $\text{H}_2\text{S}$ , at least on the order of several weeks or ideally months. Such prolonged usage involves a large number of regeneration steps, for instance in biogas facilities, and therefore we regard the accumulation of  $\text{CuSO}_4$  as a crucial challenge. Yet, the formal thermodynamic preference for  $\text{CuSO}_4$  according to Equation (2–4) based on the corresponding standard free reaction enthalpies alone is insufficient for assessing the relevance of  $\text{CuSO}_4$  for such  $\text{CuO}$ -type dosimeters: first, several other possible reactions in addition to Equation (1–3) need to be taken into account into a thermodynamic treatment. Also, the standard free enthalpy refers to a pressure of 1 bar, while under sensing conditions the partial pressures of the involved gases might be orders of magnitude different. Hence, one needs to compare free reaction enthalpies  $\Delta_r G^\circ$  as a function of the partial pressures of all gaseous components, which might be substantially different from the  $\Delta_r G^\circ$  values. Second, the kinetics of the involved reactions might have a strong influence on the reaction rates, for example preventing the formation of thermodynamically favoured compounds.

Hence, in this study we aim at elucidating the chemical parameters determining stable  $\text{H}_2\text{S}$  detection using  $\text{CuO}$  as a sensor material and particularly at addressing the  $\text{CuSO}_4$  formation and its impact on sensing. Building on such insight, we target strategies for inhibiting the  $\text{CuSO}_4$  generation. The methodology of this study was designed along the following considerations: on the one hand the copper compounds on the sensor themselves need to be studied, in order to correlate the performance of a specific sensor with possible transformations,

i.e. by studying the sensor material after different steps in the detection/regeneration cycle. On the other hand, the amount of material deposited on the sensors is so small, being below  $1 \text{ mg}$ , that standard solid-state chemical analysis (elemental analysis, X-Ray Diffraction) is not feasible to identify specific compounds. Therefore, we use Raman spectroscopy, especially a Raman microscope, as main method to determine copper compounds directly on the sensors used. A major challenge to be addressed is the determination of the significance of reaction (3) for the  $\text{CuSO}_4$  formation on the basis of the sample amounts on the sensors.

Therefore, our study is based on two conceptual methodologies. First, two types of  $\text{CuO}$  nanoparticles possessing a well-defined shape are used for sensing, and the material on the sensors is studied by post-mortem analysis by Scanning Electron Microscopy (SEM) and Raman spectroscopy. Second,  $\text{CuS}$  nanoparticles are used in sensing experiments, accompanied by ex situ oven treatment in different atmospheres corresponding to the gaseous environment surrounding the sensors. To start with  $\text{CuS}$  instead of  $\text{CuO}$  provides additional insight, as the thermal evolution of  $\text{CuS}$  represents the crucial regeneration step within the sensor cycling. Commercial and home-made spherical  $\text{CuS}$  nanoparticles of small dimension (diameter  $10\text{--}20 \text{ nm}$ ) are used, from which the impact of different interaction surface areas on the  $\text{CuSO}_4$  formation is assessed. A detailed analysis of this conversion by thermogravimetric analysis (TG) coupled with X-ray diffraction (XRD) experiments and Rietveld analysis, applying different gas atmospheres, is applied to pursue a deeper insight into the regeneration step (2). In order to understand if the different compounds possibly formed and detected follow their relative thermodynamic stability, we calculate the free reaction enthalpies  $\Delta_r G^\circ$  of various possibly relevant reactions, as function of partial pressures especially of  $\text{O}_2$  and  $\text{H}_2\text{S}$ , and for different temperatures, thoroughly taken into account the temperature-dependence of  $\Delta_r G^\circ$ .

Building on the insights obtained from these systematic analyses, we then infer strategies to prevent the formation of  $\text{CuSO}_4$ , namely by variation of the gas atmosphere, applied temperatures and times, i.e. straightforward parameters, and hence to improve the sensing performance of  $\text{H}_2\text{S}$  dosimeter-type sensors. Hence, the present study is dedicated to gain a deeper insight in the detection of  $\text{H}_2\text{S}$  with low-cost pure  $\text{CuO}$  or  $\text{CuS}$  nanomaterials on the level of the chemical conversions taking place during the sensing mechanism, aiming at improving the sensing stability in combination with good sensitivity.

## Results and Discussion

### $\text{CuO}$ nanorods - synthesis and characterization

A synthetic approach of Yang et al. is used to generate  $\text{CuO}$  nanorods with defined shape and in reproducible way.<sup>[18]</sup> Such nanorods are chosen as sensing material for two reasons. First, the loose ensemble of nanorods forms a porous network, which should enable a stable cycling behaviour over a substantial

number of sensing/regeneration cycles, as the significant morphological alterations due to the different molar volumes of CuO and CuS can be accommodated. Second, the defined particle shape allows for a straightforward detection of morphological changes, for example by scanning electron microscopy (SEM), even on the sensing substrate. The material is characterised by SEM, TEM, XRD and Raman spectroscopy.

Figure 2a) shows the XRD pattern of the CuO particles, which can be assigned to the monoclinic CuO phase (JCPDS card files no. 48-1548). No other signals are detected, indicating the product is rather pure. An average crystallite size of 27 nm is calculated by applying the Scherrer equation on the (−202) reflection, i.e. CuO is present in the form of nanocrystallites.

Raman spectroscopy analysis of the CuO particles compared to a commercial CuO material confirms that CuO is the only detected phase, in agreement with XRD (Figure 2b). Three signals are observed which can be attributed to the  $A_g$  and  $B_g$  modes of CuO, while two further signals can be assigned to the substrate.

The CuO particles (Figure 2c) possess a flat rod-like structure with an average diameter of about 50 nm and quite narrow distribution, and a length between 100 nm and 500 nm. The transmission electron microscopy (TEM) and selected area electron diffraction (SAED) patterns (Figure 2e) confirm the presence of flat CuO nanorods. Since the CuO nanorods observed by SEM and TEM are larger than the crystallite size determined by XRD, we conclude that the CuO rods consist of smaller CuO nanocrystallites. The BET area is determined by Kr physisorption and amounted to 15 m<sup>2</sup>/g, indicating no internal

porosity within the CuO nanorods. The as-prepared CuO nanorods are then studied with regard to their sensing properties towards H<sub>2</sub>S exposition.

### CuO nanorods during H<sub>2</sub>S sensing

First, the long-term stability of a sensor containing CuO nanorods is investigated. A measurement probing 10 ppm of H<sub>2</sub>S in synthetic air with 30% relative humidity is performed spanning 100 detection and regeneration cycles (Figure 3). Within this long-term measurement, the first 10 cycles are shown in detail (Figure 3b). The first marked resistance decrease above three orders of magnitude takes place in the first cycle (Figure 3b) after around 150 s. This behaviour suggests that the expected conversion of CuO to CuS takes places and a conductive path of CuS is formed. After heating up the sensor to 360 °C the conductance decreases, which is evidence for successful regeneration, i.e. the back reaction of CuS to CuO. After cycle 2, the sensor exhibits repetitive periodic conductance increases due to H<sub>2</sub>S exposition at 160 °C after similar times, and the conductance decreases upon treatment at 360 °C. After the long-term sensing measurement, the same sensor was tested in a subsequent sensing measurement in the same atmosphere in 10 sensing cycles (Figure 3c). The sensor does not show sensing activity anymore. Instead, the resistance increases in the regeneration step and decreases in the detection step, which corresponds to the typical temperature-

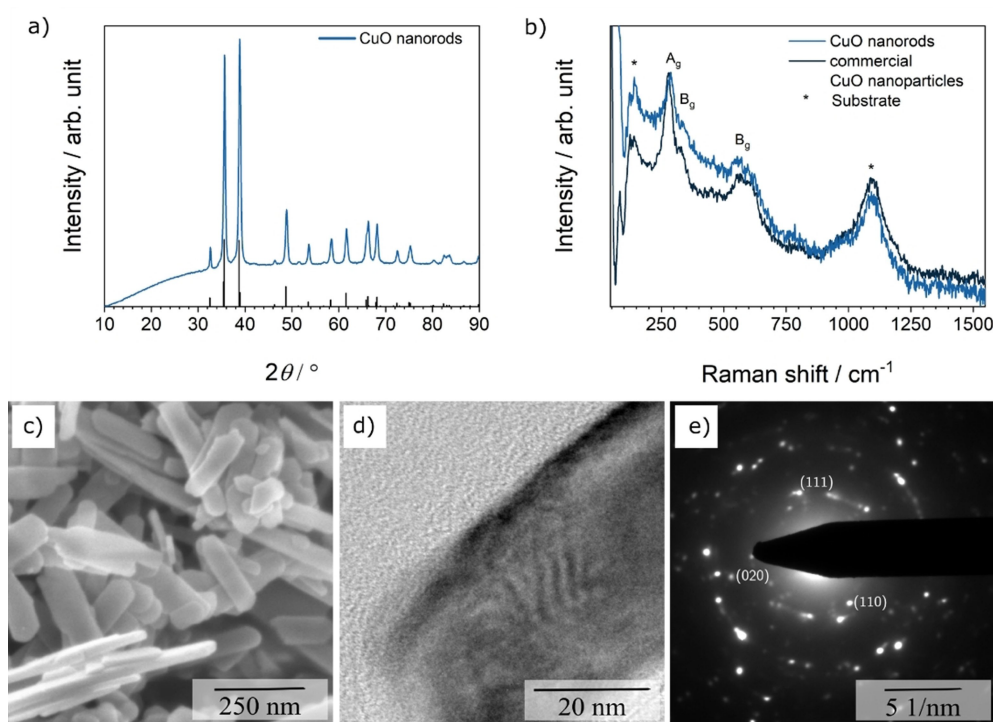


**Figure 2.** XRD pattern (a), Raman spectra (b), SEM images (c), Transmission electron microscopy (d) and the corresponding SAED pattern (e) of as-synthesized CuO nanorods.

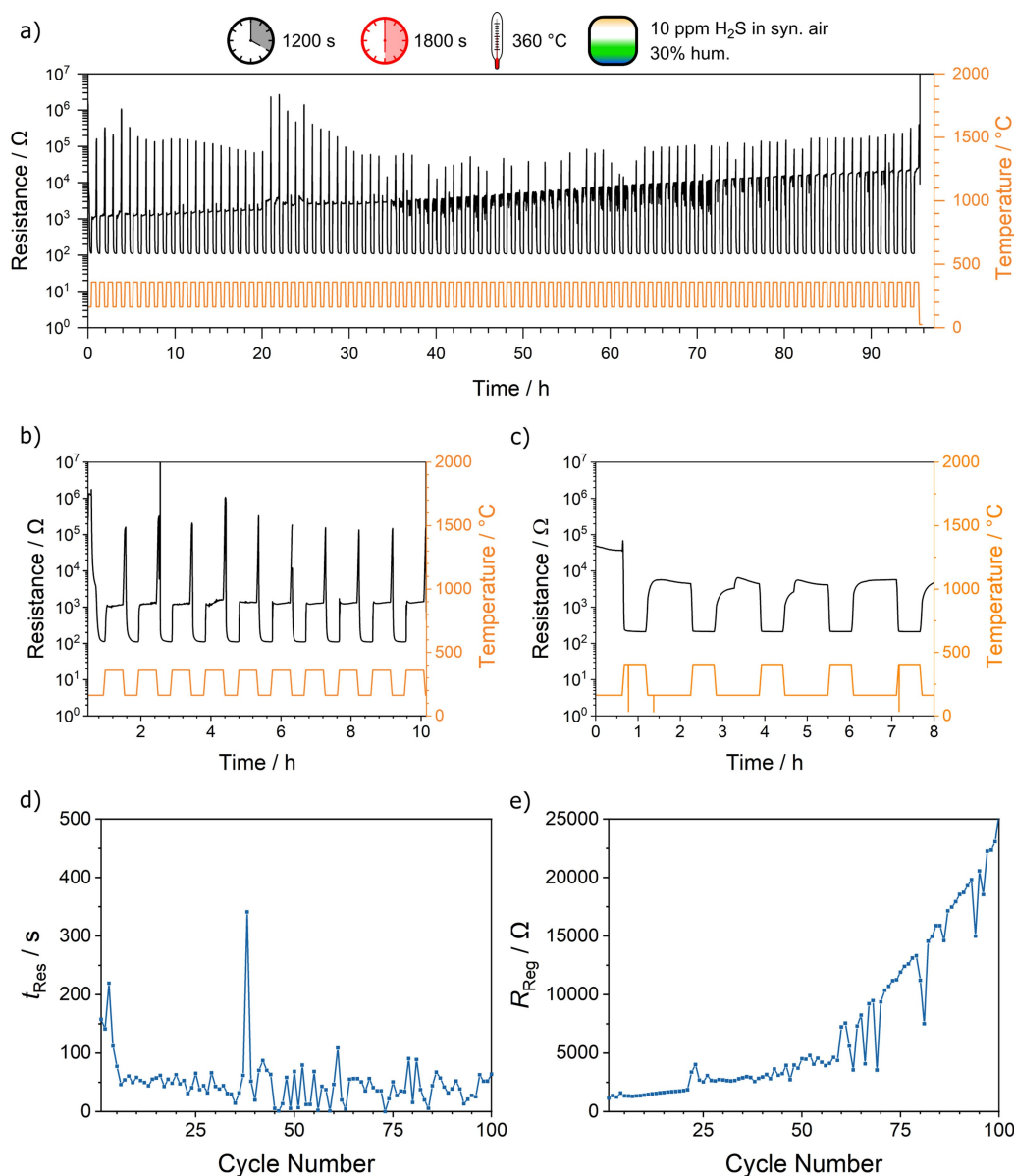


**Figure 3.** Long-term measurement with CuO nanorods on a sensor substrate applying 10 ppm H<sub>2</sub>S in synthetic air with 30% relative humidity (a) with a magnification of the first 10 cycles (b). The same sensor was tested in a subsequent sensing measurement applying the same atmosphere in 10 sensing cycles after the long-term measurement (c). Response time (d) and regeneration resistance (e) for each cycle during the long-term measurement.

dependent resistance behaviour of semiconductors, but not to the desired chemical reactions of CuO and CuS.

Additionally, an overall continuous increase in the resistance in the regeneration state by one order of magnitude is detected (Figure 3a, blue arrow). The long-term behaviour is analysed in more detail by determining two characteristic sensing parameters, the response time  $t_{\text{Res}}$  and the regeneration resistance  $R_{\text{Reg}}$  (see Figure 1). Lower gas concentrations result in longer times for building a conductive path of CuS and thus longer response times  $t_{\text{Res}}$ . The regeneration resistance  $R_{\text{Reg}}$  (Figure 1, violet circle) is mainly determined by the chemical composition of the sensing material and therefore reflects chemical alterations in the course of the regeneration. The trend of these two

characteristic sensing parameters is shown in Figure 3d)+e). After cycle 5 the sensor demonstrates reproducible response times  $t_{\text{Res}}$  of around  $50 \pm 10$  s in the first 35 cycles (Figure 3d), which is quite short and thus a practical range given the low concentration (10 ppm).

At higher cycle numbers the sensing time exhibits substantial fluctuation and a moderate increase, which is probably caused by chemical or morphological changes. Compared to  $t_{\text{Res}}$ , the  $R_{\text{Reg}}$  (Figure 3e) exhibits a substantial increase at higher cycle numbers, up to around 25000 Ω, suggesting marked alterations.

Such monotonic rise in resistance above one order of magnitude can hardly be explained in terms of the reversible

transformation between CuS and CuO or morphological changes (see Figure 4). By contrast, the formation of CuSO<sub>4</sub> is discussed as serious and disadvantageous side-reaction assuming that in the course of the sensor cycling more and more CuSO<sub>4</sub> forms, which is chemically inactive and an electric insulator.<sup>[13]</sup> Thereby, the regeneration resistance would raise during prolonged cycling, and at a certain point a high amount of CuSO<sub>4</sub> prevents the formation of a conductive path of CuS, impeding sensor activity. Still, the here-applied CuO nanorods enable the detection of 10 ppm H<sub>2</sub>S in gas dosimeter mode in 100 sensing and regeneration cycles with stable sensing times of around 50 s ± 50 s, which we attribute to the loose particle network, allowing for efficient conversion of CuO into CuS and vice versa. Compared to literature values, the variations and sensing times are thus in a similar range.<sup>[19]</sup> In this respect, the use of CuO nanorods seems to be a promising concept in H<sub>2</sub>S sensing, but the longevity and the cycling stability represents a major and fundamental obstacle. In order to elucidate the decrease in sensing performance in relation to chemical transformations, we investigate the sensing material during the different parts of one cycling period and after prolonged cycling in fine detail, which is described in the following.

After different steps during the cycling experiment, the sensor is analysed by SEM and Raman spectroscopy measurements (Figure 4). Note that these analyses are conducted on the very same material used on the sensor device, i.e. these characterizations can be regarded as a post-mortem analysis and thus reveal the state of the material on the sensor.

In the initial state, the sensing material consists of well-defined CuO nanorods (Figure 4 a), which were then heated up to 160 °C and exposed to 10 ppm H<sub>2</sub>S.

At a certain time, a conductive path of CuS is formed and the resistance decreases by more than one order of magnitude (Figure 4b, after first detection). The SEM image (Figure 4b) performed on the samples after the first detection step does not reveal any significant morphological deformation; nanorods with similar dimensions and morphology compared to the initial state can be observed and Raman spectroscopy reveals solely the signals of CuO. Although the decrease in resistance is certainly due to a network of conductive paths beyond the percolation threshold, CuS is not detected by Raman spectroscopy, probably because the amount formed during the first sensing cycle is below the detection limit of the Raman spectrometer, and the conductive CuS path is formed only on the particle surface. In the next step the sensor is heated up to 360 °C for regeneration, causing the back reaction from CuS to CuO, and after cooling down to 160 °C the resistance turns back to the initial state (Figure 4c). During this regeneration step, the morphology of the sensing material changes significantly, as seen by aggregated rods, but retaining their shape. The Raman spectroscopy measurement (Figure 4c, right) indicates a complete chemical transformation into CuO. During the next detection step (Figure 4d), the morphology of the sensing material undergoes a continuous change, with SEM revealing a rough surface consisting of small particles, speaking for substantial chemical transformation.

The material shows marked morphological changes, and Raman spectroscopy now reveals three different compounds: next to CuO, the signal at 470 cm<sup>-1</sup> indicates CuS, and additionally CuSO<sub>4</sub> is detected. Being an insulator, continuously generated CuSO<sub>4</sub> results in an increase in the  $R_{\text{Reg}}$ . However, despite side reactions such as the formation of CuSO<sub>4</sub> during detection or regeneration, a sufficient amount of CuO remains for the detection of H<sub>2</sub>S, as demonstrated in Figure 4e), presenting SEM and Raman spectroscopy analyses after 10 sensing and detection cycles. SEM indicates that particles located on the nanorods grow and the amount of CuSO<sub>4</sub> increases as well suggesting that these particles can be interpreted as CuSO<sub>4</sub> on the particles' surface. A small signal ascribed to CuS is still visible in Raman spectroscopy, further indicating that CuS cannot be fully converted to CuO (or Cu<sub>2</sub>O) during regeneration steps.

These studies also unveil that CuS accumulates in the sensing material in the course of multiple sensing cycles, but the degree of conversion of CuS still is sufficient for the breakdown of the conductive path, as seen by the steep increase in resistance in each step. Yet, such leftovers of CuS as well as CuSO<sub>4</sub> can be a reason for the stark fluctuation in switching time in higher cycling numbers (Figure 3d). On the one hand, the accumulation of CuSO<sub>4</sub> on the particles' surface hinders the formation of a conductive path and hence the response time increases. On the other hand, non-regenerated CuS paths leads to smaller switching times in a subsequent H<sub>2</sub>S exposure. The measurements and analyses after 100 sensing cycles (Figure 4f) confirm these trends: the rod-like particle structures have disappeared, and CuS and CuSO<sub>4</sub> accumulate in the sensing material. Since the morphology change and the CuS accumulation should not lead to a breakdown of the sensor even after 100 sensing cycles, it is rather the continuous formation of chemically inactive CuSO<sub>4</sub> which reduces sensing activity after repeated cycling.

In order to further verify the role of CuSO<sub>4</sub> and to exclude a strong impact of the morphology of CuO, in a second set of experiments such measurements are performed using isotropic CuO nanoparticles, possessing a relatively high BET area of 120 m<sup>2</sup>/g (Figure S1). Compared to the CuO nanorods, these CuO nanoparticles undergo a much more severe morphological transformation, and substantial formation of CuSO<sub>4</sub> can be observed during the sensing measurements, disturbing and finally eliminating sensing activity in lower cycle numbers compared to CuO nanorods. The more drastic changes can be attributed to the larger surface area, which apparently spurs the formation of CuSO<sub>4</sub>. In summary, this comparison suggests that the ongoing accumulation of CuSO<sub>4</sub> is the main problem in the long-term H<sub>2</sub>S sensing using CuO materials. Hence, any CuO material should be usable for detecting H<sub>2</sub>S in the dosimeter mode, as long as the formation of a continuous path is possible, i.e. as long as the amount of CuSO<sub>4</sub> remains small. Thus, in the following the formation of CuSO<sub>4</sub> is subjected to detailed investigation, finally aiming at a strategy to prevent excessive CuSO<sub>4</sub> formation and thus for a stable H<sub>2</sub>S dosimeter-type sensor enabling long-term usage.



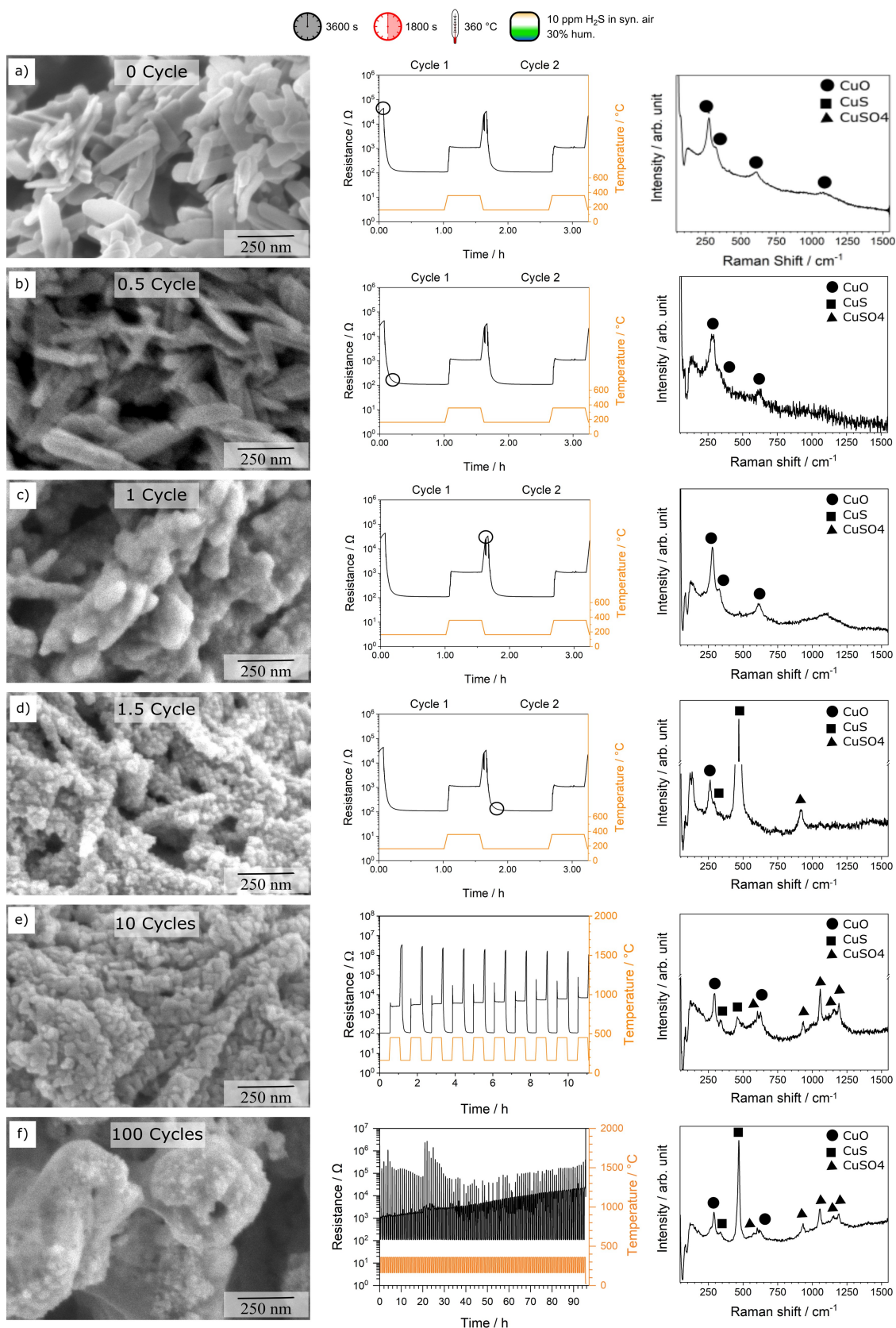
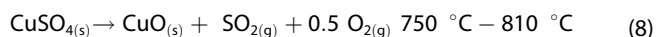
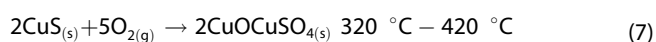
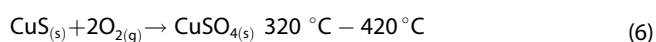
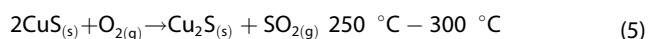


**Figure 4.** Detailed analyses of H<sub>2</sub>S sensing using CuO nanorods applying SEM (first column) and Raman spectroscopy (third column) measurements. Different states during the sensing cycles were investigated: initial state (a), after first detection (b), after first regeneration (c), after second detection (d), after 10 cycles (e) and after 100 cycles (f). The second column illustrates the state during cycling at which SEM and Raman spectroscopy was performed on the material used on the sensor device.

In-depth investigation of CuSO<sub>4</sub> formation

Assuming, that the decrease in H<sub>2</sub>S sensing performance is mainly attributable to the regeneration step, which ideally starts from CuS (or possibly from Cu<sub>2</sub>S), commercial CuS nanoparticles are heated up in air with 30% relative humidity up to 1000 °C, and the accompanying chemical transformations are studied by TG coupled with mass spectrometry (TG-MS) and XRD. The XRD data are analysed by Rietveld refinement, thus providing the fraction of possible reaction products such as CuO, Cu<sub>2</sub>O, CuSO<sub>4</sub>, etc. (Figure 5). In the TG-MS experiment (Figure 5a), the relative mass stayed constant until 300 °C. Subsequently, a mass loss of around 15% takes place up to 400 °C. Reaching ca. 550 °C, the sample mass shows an increase of around 40% staying constant until the temperature reaches around 700 °C. Afterwards, the mass declines by around 40% and reaches the final relative mass of 85% in relation to the initial mass, at around 800 °C. By heating up to 1000 °C, no further changes take place. A similar behaviour was reported in literature.<sup>[20]</sup>

The first decrease in relative mass can be correlated to the formation of copper(I)sulfide Cu<sub>2</sub>S (see reaction 5). By further heating (320 °C – 420 °C) CuSO<sub>4</sub> and copper(II)oxysulfate (CuOCuSO<sub>4</sub>) are formed resulting in an increase in relative mass (6 + 7). Above 750 °C the reaction to CuO takes place (8).



In order to further elucidate the composition, we carry out XRD measurements of CuS heated up in a separate oven and exposed to synthetic air with 30% relative humidity (Figure 5c). Note that the minute sample amount usually put on the sensors does not allow for studying this very same material by XRD, as larger quantities (i.e. ca. 100 mg) are required to obtain meaningful quantitative XRD analyses.

The phase compositions calculated by Rietveld refinement confirm the observations from literature.<sup>[20]</sup> Below 300 °C, only CuS and a small amount of Cu<sub>1.8</sub>S are detected. Between 300 °C and 350 °C, the reactions (4) and (5) take place and indeed Cu<sub>1.8</sub>S, Cu<sub>2</sub>S and CuSO<sub>4</sub> are observed. At higher temperatures (450 °C and 550 °C), the complete decomposition of CuS and Cu<sub>2</sub>S takes place and result in a mixture of CuSO<sub>4</sub>, CuOCuSO<sub>4</sub> and CuO. The amount of CuOCuSO<sub>4</sub> increases at 550 °C compared to 450 °C. Above 800 °C, CuSO<sub>4</sub> decomposes completely and CuO is formed. Thus, it appears that on such macroscopic scale, i.e. using CuS powders, the regeneration temperature (350 °C) is insufficient for the formation of CuO, as only at 450 °C a small amount of CuO forms during regeneration, and even higher temperatures (800 °C) are required for obtaining CuO. Yet, the sensor substrates do not withstand such high temperatures upon prolonged cycling, and the thermal stress could result in further problems in cycling

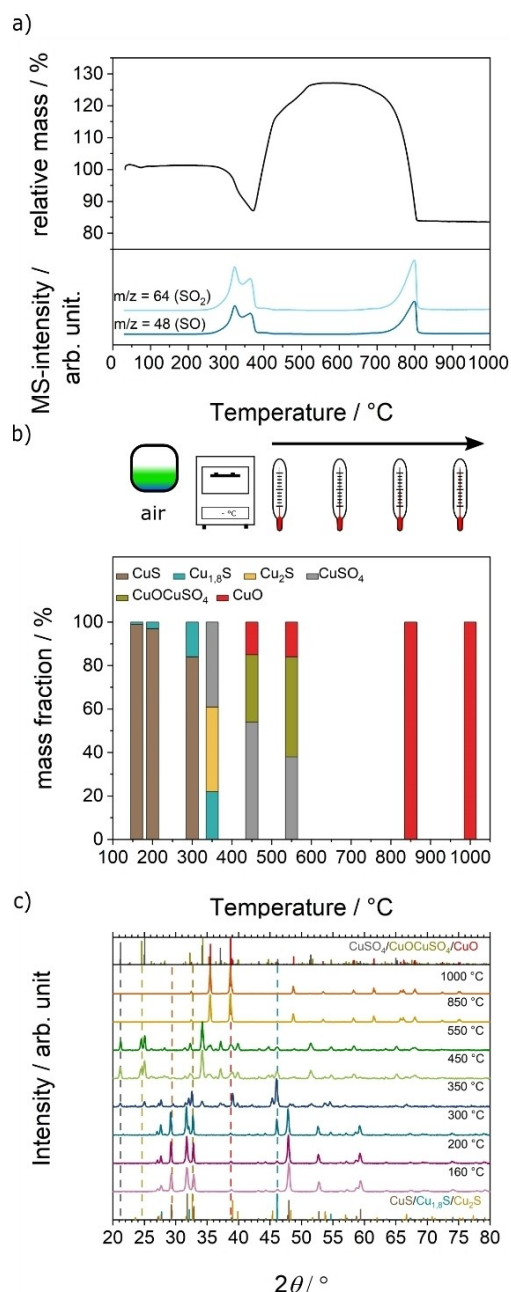


**Figure 5.** TG measurement (in air) coupled with MS of commercial CuS (a) and compositions (b) determined from XRD data with reference (reference database see supporting Information file) (c) after heating up CuS to elevated temperatures corresponding to chemical transformations according to the TG measurement.

stability. Hence, based on these insights, we decide to heat the sensors to 450 °C instead of 350 °C in the regeneration step and checked the applicability of commercial CuS as sensor material, instead of CuO. Such CuS-based sensor indeed exhibits a well-defined and stable sensing behaviour over ten sensing and regeneration cycles (Figure S2), proving the reversible formation of a sufficient amount of CuO.

In order to clarify the impact of the morphology of the used CuS material, additionally small CuS nanoparticles (below



20 nm in diameter, Figure 6b) are prepared by a recently optimized low-temperature synthesis<sup>[21]</sup> (see Experimental Section) and tested in sensing experiments (Figure 6c + d) under the same conditions as the commercial CuS nanopowder. The nanoparticles exhibit a well-defined ellipsoidal shape and a significantly larger BET surface area (35 m<sup>2</sup>/g), and hence should result in a faster kinetics of the aforementioned relevant reactions. These nanoparticles consist of a mixture of CuS and Cu<sub>1.8</sub>S, as revealed by XRD, and interestingly exhibit the same sensing behaviour as the commercial CuS material, which means that Cu<sub>1.8</sub>S exerts no significant impact on sensing properties. This material shows stable sensing behaviour in 20 sensing and regeneration cycles, too (Figure 6c). Hence, during regeneration sufficient CuS is decomposed and a sufficient amount of CuO is formed for the detection of H<sub>2</sub>S in a next cycle. Yet, the regeneration resistance increases as well (Figure 6d), indicating the accumulation of CuSO<sub>4</sub> in these measurements. The regeneration of these particles also is investigated by TG-MS and oven experiments combined with XRD measurements (Figure S3), both performed in air, revealing a similar behaviour as commercial CuS with the exception of two significant differences. There is no steep mass loss visible in the TG-MS measurement at around 350 °C. Due to the presence of Cu<sub>1.8</sub>S already in the initial sample the formation Cu<sub>1.8</sub>S and

Cu<sub>2</sub>S via reaction (5) is less pronounced at temperatures between 100 °C and 300 °C. Additionally, a small amount of CuO is present at 350 °C, probably because the small size and the higher BET area of the CuS nanoparticles result in a shift of the reactions to lower temperatures.

In order to rationalize and understand the generation of CuSO<sub>4</sub> and other compounds as a function of the regeneration temperature in terms of thermodynamics, the standard free reaction enthalpy  $\Delta_R G^\circ$  is calculated for those reactions being relevant in the regeneration step as suggested by the TG-MS analysis, for temperatures of 350 °C and 450 °C (Eq. (5)–(7)). In the calculations of  $\Delta_R G^\circ$ , using the Gibbs-Helmholtz equation  $\Delta_R G^\circ = \Delta_R H^\circ - T \Delta_R S^\circ$ , the temperature dependence of the reaction enthalpies and reaction entropies are taken into account. (Table 1, see Supporting Information file for details of the calculation).

The formation of CuSO<sub>4</sub> and CuOCuSO<sub>4</sub> is highly exergonic and the  $\Delta_R G^\circ$  values are much more negative than for the reaction from CuS directly to CuO (7). By contrast, the decomposition of CuSO<sub>4</sub> to CuO is endergonic. At higher temperature (450 °C), the  $\Delta_R G^\circ$  values change compared to the standard regeneration temperature (350 °C), of course strongly depending on the magnitude of the entropy term in the Gibbs-Helmholtz equation. Note that the differences in  $\Delta_R G^\circ$  among

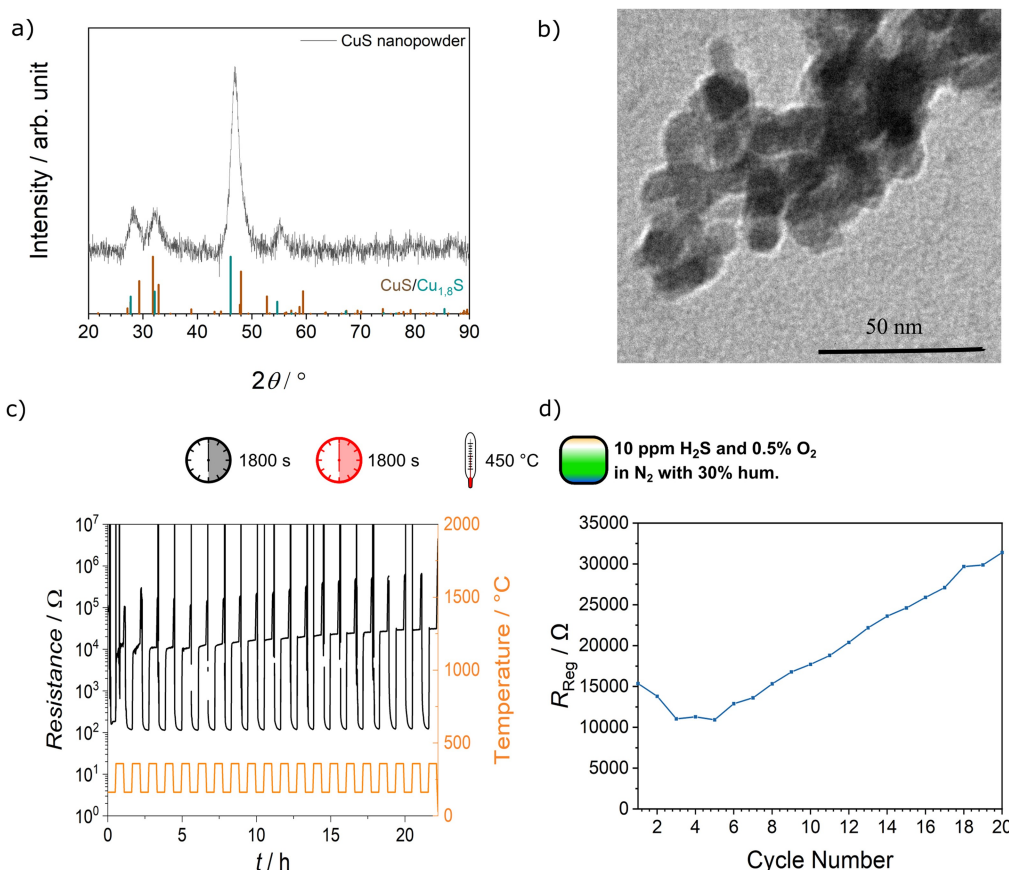


**Figure 6.** XRD (a) and TEM (b) measurement of CuS nanoparticles prepared by a low temperature method. Sensing measurement with these CuS nanoparticles on a sensor substrate applying a regeneration temperature of 450 °C in 10 ppm H<sub>2</sub>S in synthetic air with 30% humidity (c) and response time (d) for each cycle during the measurement.

**Table 1.** Standard free enthalpy  $\Delta_R G^\circ$  calculated for the regeneration reactions (2) and (5–8) by the Gibbs-Helmholtz equation for 350 °C and 450 °C, taking into account the temperature dependence of the reaction enthalpies and reaction entropies (see Supporting Information).

Reaction	$\Delta_R G^\circ$ (350 °C) [kJ mol <sup>-1</sup> ]	$\Delta_R G^\circ$ (450 °C) [kJ mol <sup>-1</sup> ]
$\text{CuS}_{(s)} + 1.5 \text{O}_{2(g)} \rightarrow \text{CuO}_{(s)} + \text{SO}_{2(g)}$	-344	-334
$2\text{CuS}_{(s)} + \text{O}_{2(g)} \rightarrow \text{Cu}_2\text{S}_{(s)} + \text{SO}_{2(g)}$	-288	-290
$\text{CuS}_{(s)} + 2\text{O}_{2(g)} \rightarrow \text{CuSO}_{4(s)}$	-488	-450
$\text{Cu}_2\text{S}_{(s)} + 2.5\text{O}_{2(g)} \rightarrow \text{CuOCuSO}_{4(s)}$	-549	-501
$\text{CuSO}_{4(s)} \rightarrow \text{CuO}_{(s)} + \text{SO}_{2(g)} + 0.5 \text{O}_{2(g)}$	+140	+112

the reactions are still significant also at 450 °C. While in principle the product composition might also be determined by kinetic effects, these substantial differences in  $\Delta_R G^\circ$ , favouring Cu sulfates from a thermochemical point of view, are in good conformity with the composition as determined by XRD (see Figure 5). This good agreement is reasonable as these elevated temperatures allow activation barriers to be overcome, which leads to the equilibrium composition. However, as the temperature stability of typical low-cost sensor substrates is quite limited, applying sufficiently high regeneration temperatures, spurring the decomposition of  $\text{CuSO}_4$  into  $\text{CuO}$ , does not appear as a feasible strategy towards a sensor with long-term cycling stability.

Also, the composition of the atmosphere is an important parameter affecting the generation of  $\text{CuSO}_4$ : small concentrations of oxygen should, along the theory of chemical equilibrium as well as kinetics, suppress the formation of copper sulfate compounds. In order to further elucidate the impact of the gas composition on the  $\text{CuSO}_4$  formation, the dependency of  $\Delta_R G^\circ$  for several relevant reactions involving CuS on the partial pressures are calculated using the well-known relationship (9), assuming that the activities  $a_i$  can be replaced by  $p_i/p_0$  of the involved gases i:

$$\Delta_R G(p) = \Delta_R G^\circ + RT \ln \frac{[p_C/p^0]^{v_C} [p_D/p^0]^{v_D}}{[p_A/p^0]^{v_A} [p_B/p^0]^{v_B}} \quad (9)$$



For example, for reaction (6) the dependence of  $\Delta_R G$  on the partial pressure of oxygen  $p(\text{O}_2)$  is given by

$$\Delta_R G(p_{\text{O}_2}) = \Delta_R G^\circ + RT \ln \frac{1}{[p_{\text{O}_2}/p^0]^2} \quad (11)$$

For the reactions generating  $\text{SO}_2$ , the value of the relative pressure  $p(\text{SO}_2)$  to be entered in the corresponding Equation (9) is, unfortunately, too small to be determined and thus as a quite small constant value ( $p(\text{SO}_2) = 10^{-10}$  bar) is chosen for the respective equations, as  $\text{SO}_2$  generated in the experiment is constantly removed by the applied gas flow. The calculation of  $\Delta_R G$  of the reactions (2) and (5)–(7) as a function of  $p(\text{O}_2)$ , for 350 °C, reveals interesting trends (Figure 7a). In ambient atmosphere, i.e. for  $p(\text{O}_2) \approx 0.19$  bar, the reactions leading to  $\text{CuSO}_4$  or  $\text{CuOCuSO}_4$  are clearly thermodynamically favoured, as

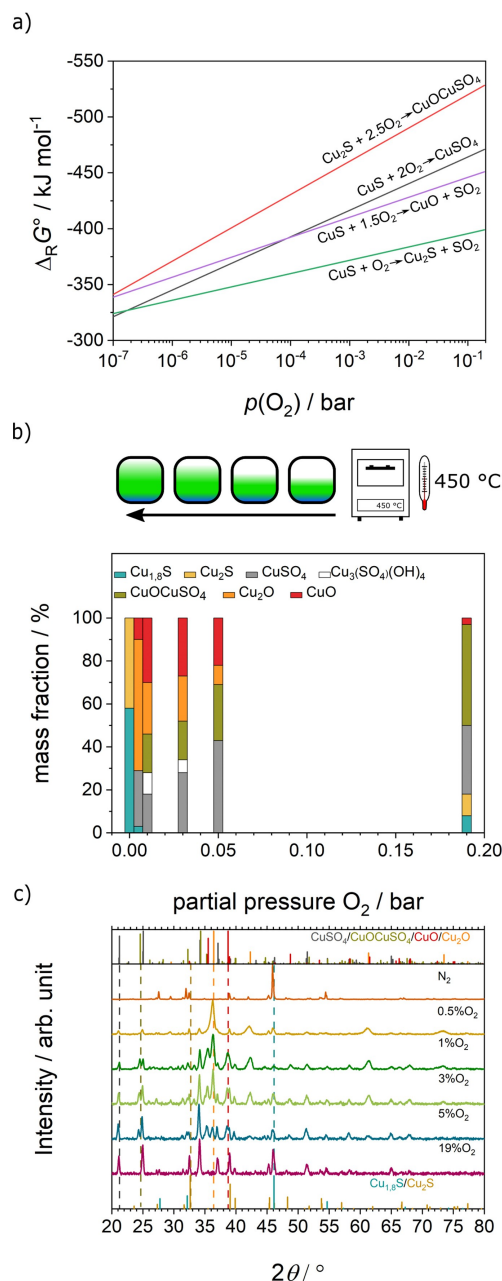


**Figure 7.**  $\Delta_R G$  values of relevant regeneration reactions depending on the partial pressure of  $\text{O}_2$  at 350 °C (a) and compositions (b) determined from XRD data with reference (reference database see supporting Information) (c) after heating up CuS to 450 °C in atmospheres with reduced partial pressure of  $\text{O}_2$ .

seen by the lowest  $\Delta_R G$  values. By contrast, with decreasing  $p(\text{O}_2)$  the free reaction enthalpies of the different regeneration reactions increase and converge. At very low pressures ( $< 10^{-7}$  bar)  $\Delta_R G$  of the formation of  $\text{CuO}$  from  $\text{CuSO}_4$  (Eq. (8)) even exceeds those of the other reactions and the formation of  $\text{CuO}$  should be preferred, which is in agreement with the principle of Le Chatelier. Applying the higher regeneration temperature (450 °C) shows a similar trend (Figure S4).

Consequently, based on these calculations (Figure 7a), it should be possible to reduce the amount of  $\text{CuSO}_4$  by reducing the partial pressure of  $\text{O}_2$ , which is experimentally tested by heating up commercial  $\text{CuS}$  to  $450^\circ\text{C}$  in atmospheres with  $p(\text{O}_2)$  ranging between 0 bar and 0.19 bar. The resulting compositions are investigated by XRD measurements (Figure 7b) followed by Rietveld analysis (Figure 7c). The experimentally determined compositions are qualitatively in excellent agreement with the  $\Delta_r G$  calculations (Figure 7c): by decreasing

$p(\text{O}_2)$  to as low as 0.005 bar, the amount of  $\text{CuSO}_4$  and  $\text{CuO}\cdot\text{CuSO}_4$  decreases and even vanishes, while the fractions of  $\text{CuO}$  and  $\text{Cu}_2\text{O}$  raise. Heating experiments without any  $\text{O}_2$  result in a mixture of  $\text{Cu}_{1.8}\text{S}$  and  $\text{Cu}_2\text{S}$  as expected.  $\text{Cu}_2\text{O}$  might be converted into  $\text{CuO}$  applying a second heating step with increased  $p(\text{O}_2)$ . Building on this insight, a sensor measurement was conducted applying a reduced amount of oxygen (0.5%) in the gas flow (Figure 8).

The material shows a stable sensing behaviour in 10 sensing and regeneration cycles (Figure 8a), and after the regeneration step of the tenth cycle the Raman spectroscopy data show no other signals beside  $\text{CuO}$  (Figure 8b). These promising cycling tests prove it is possible to suppress the formation of detrimental  $\text{CuSO}_4$  by using a low atmospheric  $\text{O}_2$  concentration. The reduced amount of oxygen has no influence on the quality on the sensing behaviour, providing a strategy for a long-lasting  $\text{H}_2\text{S}$  sensor, for example by exposing the sensor to an oxygen-deficient atmosphere in the regeneration step. Yet, the application of an atmosphere with low  $p(\text{O}_2)$  might be technically unpractical. However, these experiments studying the heterogeneous reaction of copper compounds under variation of temperature and gas atmosphere clearly give insight which can be transferred to optimize the sensor performance.

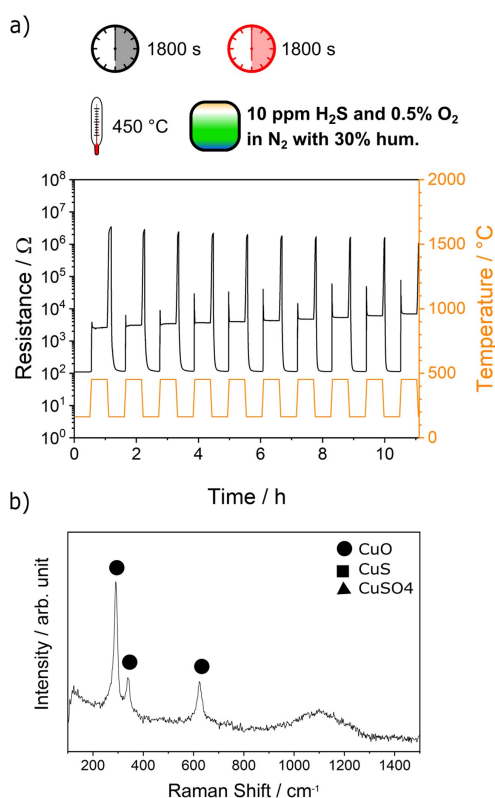


**Figure 8.** Sensing measurement with  $\text{CuO}$  nanorods on a sensor substrate applying a reduced amount of oxygen (10 ppm  $\text{H}_2\text{S}$  and 0.5%  $\text{O}_2$  in  $\text{N}_2$  with 30% hum) (a) and a Raman spectroscopy measurement of the sensing material after ten cycles (b).

### Optimization of sensing settings

In spite of the promising sensing and stability properties, the variation of atmospheric composition is not feasible for practicable application of these sensors. Therefore, alternatively we study modified sensing settings to improve the sensing stability, a summary of which is shown in Figure 9, applied on  $\text{CuO}$  nanorods.

For each variation, a measurement with 10 sensing and regeneration cycles was performed coupled with Raman spectroscopy analysis of the sensing material after completion of the respective sensing tests, i.e. stopping after a regeneration step.

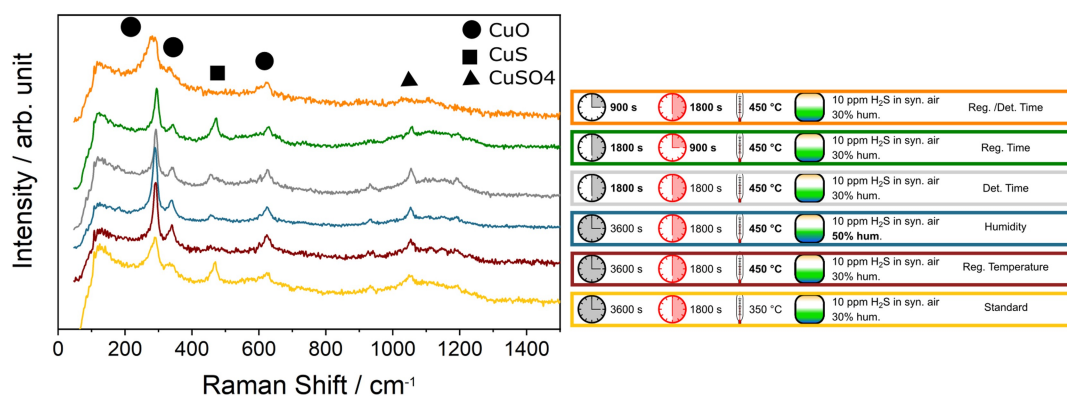


**Figure 9.** Raman spectroscopy measurements of sensor substrates after measuring  $\text{H}_2\text{S}$  in 10 sensing and regenerations cycles under variation of technical settings, namely time, temperature and humidity.

First, the measurement is conducted using standard settings (i.e. a volume fraction of oxygen of 20 %) serving as a reference in this series (Figure 9, yellow curve). Indeed,  $\text{CuSO}_4$  is formed and  $\text{CuS}$  is not completely converted into  $\text{CuO}$ . By raising the regeneration temperature to 450 °C, whilst keeping the same atmosphere,  $\text{CuSO}_4$  is still formed during sensing measurement.

However, the  $\text{CuS}$  signal disappears, which means that this higher temperature results in a complete decomposition of  $\text{CuS}$  during regeneration indicating the formation of an increased amount of  $\text{CuO}$ . Therefore, the elevated regeneration temperature of 450 °C is used in the subsequent sensing experiments. In the next experiment (Figure 9, blue curve) the relative humidity is increased to 50 %, without a significant effect on the Raman spectroscopy pattern and sensing (Figure S5). It is therefore possible to detect  $\text{H}_2\text{S}$  in an environment with higher relative humidity, but the  $\text{CuSO}_4$  formation and sensing behaviour are unaffected. Repeated sensing experiments in atmospheres with high relative humidity values (50 % and 80 %) are possible (Figure S6). The material shows the typical sensing behaviour with stable sensing and regeneration cycles (Figure S6). Subsequently, the detection and regeneration times are decreased to  $t_{\text{Detect}} = 1800$  s (detection) and  $t_{\text{Reg}} = 900$  s (regeneration) (Figure 9, green curve).  $\text{CuSO}_4$  is still visible in the Raman spectroscopy data, and the signal of  $\text{CuS}$  reappears after the measurement. Thus, a regeneration time of  $t_{\text{Reg}} = 900$  s is insufficient for the complete decomposition of  $\text{CuS}$ , which is formed during cycling with  $t_{\text{Detect}} = 1800$  s. Next, the regeneration time  $t_{\text{Reg}}$  is increased to 1800 s and  $t_{\text{Detect}}$  is decreased to 900 s (Figure 9, orange curve). Interestingly, after ten sensing cycles pure  $\text{CuO}$  is present after the measurement, owing to a

complete decomposition of  $\text{CuS}$  without the emergence of  $\text{CuSO}_4$ . Hence, as an important finding, the amount of formed  $\text{CuSO}_4$  during 10 sensing cycles can be decreased by reducing  $t_{\text{Detect}}$  without changing  $t_{\text{Reg}}$ . Certainly, for lower concentrations the detection and regeneration time have to be adjusted, due to the decrease in response time for lower  $\text{H}_2\text{S}$  concentrations.

Building on this promising insight, these optimized sensing parameters are used in a long-term sensing measurement with  $\text{CuO}$  nanorods, i.e. applying  $t_{\text{Detect}} = 900$  s as detection time,  $t_{\text{Reg}} = 1800$  s and a regeneration temperature of 450 °C in 10 ppm  $\text{H}_2\text{S}$  in synthetic air with 30 % relative humidity.

The sensing material now shows a stable sensing pattern in over 250 detection and regeneration cycles (Figure 10). In nearly each cycle the resistance decreases over several orders of magnitude due to the formation of a conductive path of  $\text{CuS}$  and significantly increases afterwards because of the regeneration at 450 °C. Notably, this sensor also demonstrates reproducible response times of around 100 s (Figure 10b). At higher cycle numbers the variations in  $t_{\text{Res}}$  increase due to chemical or morphological changes. The regeneration resistance (Figure 10c) exhibits an increase in resistance from 2500  $\Omega$  to 12500  $\Omega$  during the measurement. Compared to the previously applied setting, featuring a longer detection time, the increase in resistance during the whole measurement is smaller and the sensing material exhibits a stable sensing behaviour in a larger number of cycles.

These observations therefore indicate a reduced formation of  $\text{CuSO}_4$  during the measurement. By decreasing the detection time, a reduced amount of  $\text{CuS}$  is formed during the detection mode, in turn resulting in a decreased formation of  $\text{CuSO}_4$ .

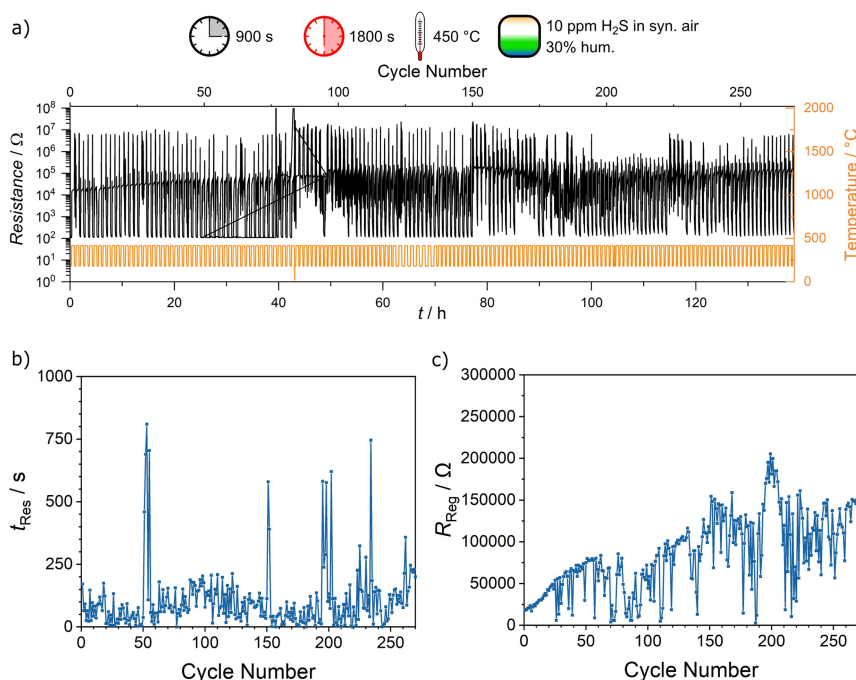


**Figure 10.** Long-term measurement with  $\text{CuO}$  nanorods on a sensor substrate applying 10 ppm  $\text{H}_2\text{S}$  in synthetic air with 30 % relative humidity, 900 s sensing time, 1800 s regeneration time and a regeneration temperature of 450 °C (a). Response time (b) and regeneration resistance (c) for each cycle during the long-term measurement.

during regeneration. Therefore, a shorter detection time coupled with a higher regeneration temperature result in an increased stability with a sensing activity in over 250 cycles. Certainly, the formation of  $\text{CuSO}_4$  cannot be entirely prevented, as described in the previous section, but the sensing stability can be improved significantly by optimizing these sensing settings.

## Conclusion

The use of CuO materials for  $\text{H}_2\text{S}$  dosimetry, exploiting the formation of conductive CuS/Cu<sub>2</sub>S paths and the steep increase in conductance when the percolation threshold is reached, is a potentially feasible sensor concept. In principle, this type of CuO sensors allows for long-term and low-cost dosimetric detection of  $\text{H}_2\text{S}$ , even for low concentrations in the range of the maximum allowed exposure limits, i.e. 5 ppm or 10 ppm. Yet, the occasionally observed continuous decay in the sensing performance under permanent exposure to  $\text{H}_2\text{S}$  is a hindrance. Here we focus the underlying chemical reactions during sensing to improve the long-term stability of these sensors.

As main conceptual methodology we used CuO nanorods of well-defined shape and studied chemical and morphological alterations at the different steps of the sensing cycles (see Figure 1), in order to identify the process(es) resulting in loss in sensing performance. While the morphological were easily detectable by SEM images of the material deposited on the sensor, the composition of the solid material was analysed by Raman spectroscopy on the very same sensor. Together with the corresponding sensor signal, we were thus able to correlate the conductance with both, morphological and chemical transformations on one particular sensor. As main result from this concerted elaborate analysis, we conclude that the formation of  $\text{CuSO}_4$  occurs predominantly during the regeneration step, i.e. during heating CuS under atmosphere conditions. As such on-the-sensor analysis can hardly quantify the composition, CuO and CuS were heated under controlled conditions (temperature, gas composition) in an oven, enabling larger sample quantities and thereby quantitative analysis by XRD, providing the exact composition by Rietveld refinement. These experiments were confirmed with calculation of the Gibbs Free Enthalpy of various possible reactions. Indeed, experimental analysis and thermodynamics consistently prove the dilemma that not CuO, but  $\text{CuSO}_4$  is favoured under these conditions, thereby counteracting the reusability of such sensors. In essence, our study proves that extensive, irreversible formation and accumulation of  $\text{CuSO}_4$  is a chemical process leading to continuous decline in sensing performance, as  $\text{CuSO}_4$  is an insulator.

Building on this insight, we concluded that a chemical strategy avoiding the  $\text{CuSO}_4$  formation must take advantage of kinetics as well. Hence, keeping other sensing parameters constant, we reduced the detection time shorter detection time coupled with a higher regeneration temperature result. Indeed, less  $\text{CuSO}_4$  was generated, on the one hand because of the shorter time for converting CuS into  $\text{CuSO}_4$ , and on the other hand the formation of  $\text{CuSO}_4$  thermodynamically is less

preferential at elevated temperature. The concept to minimize  $\text{CuSO}_4$  formation in terms of a kinetic principles is supported by the observation that CuS nanoparticles, possessing an overall high surface area undergo a more severe decline after a series of sensing cycles. Evidently, a higher interaction area between CuS and the oxygen-containing atmosphere is detrimental, resulting in a higher reaction rate of the CuS oxidation. We would like to note that this result also shows that a nano-structure is not always beneficial for sensing. Instead, for CuO-based dosimetry the particles should rather be of a dimension beyond the nanoscale.

Based on these systematic studies, finally  $\text{H}_2\text{S}$  sensors based on CuO nanorods with a stable sensing behaviour in more than 250 detection cycles can be achieved. This advancement was possible by approaching the sensing problems from a chemical point of view, which is translated into a longer lifetime of the sensor.

Hence, our study demonstrates that rigorous analysis of the chemical reactions taking place between solids and gases provides distinct inside into the failure of CuO-based dosimeters. Guided by general principles of kinetics and thermodynamics it is possible to reduce the formation of detrimental  $\text{CuSO}_4$  and thus to substantially improve the life-time and thus overall sensing performance. We believe that this conceptual methodology might be applied to advance the performance of other types of dosimeters building on chemical transformations.

## Experimental Section

**Chemicals:** All chemicals are of analytical grade and used as received: copper(II)acetate-monohydrate ( $\text{Cu}(\text{OAc})_2 \cdot \text{H}_2\text{O}$ , Sigma Aldrich), copper(II)nitrate-trihydrate ( $\text{Cu}(\text{NO}_3)_2 \cdot 3 \text{H}_2\text{O}$ , Sigma Aldrich), copper(II)chloride-dihydrate ( $\text{CuCl}_2 \cdot 2 \text{H}_2\text{O}$ , Sigma Aldrich), sodium sulfide-nonahydrate ( $\text{Na}_2\text{S} \cdot 9 \text{H}_2\text{O}$ , Alfa Aesar), deionized water ( $\text{H}_2\text{O}$ ) and ethanol (EtOH, Fisher Scientific).

**CuO nanorod preparation:** The CuO nanorods are prepared by a hydrothermal approach reported by Yang et al.<sup>[18]</sup> First a solution of 0.5 M copper(II)nitrate in absolute ethanol is prepared. Subsequently this solution (5 mL, 2.5 mmol  $\text{Cu}(\text{NO}_3)_2$ ) is added to 10 M sodium hydroxide solution (10 mL, 0.1 mol NaOH). The mixture is transferred into a Teflon-lined hydrothermal synthesis autoclave (45 mL, Parr Instrument Company, Model 4744 General Purpose Acid Digestion Vessel) and treated for 12 h in a drying oven at 100 °C. Afterwards, the particles are separated via centrifugation (7500 rpm) and washed three times with demineralized water and three times with ethanol. Finally, the dark brown powder is dried at 60 °C in a vacuum oven for 3 h. Characterization is performed with a “Merlin” instrument by Zeiss for scanning electron microscopy (SEM) images and a Philips CM30 instrument equipped with a LaB6 cathode (300 kV) for transmission electron microscopy (TEM). X-ray diffraction (XRD) measurements are performed with a X’Pert Pro from PANalytical using  $\text{CuK}\alpha$  radiation for and a step size of  $2\theta = 0.026^\circ$ , and a time per step of 150 s in a range of  $2\theta = 10\text{--}90^\circ$  and a “Senterra” Raman microscope from Bruker with a 532 nm laser was used for Raman measurements.

**Synthesis of CuS nanoparticles:** The CuS nanoparticles are prepared by adapting a low-temperature batch method.<sup>[21]</sup> First a 0.1 M aqueous copper(II)chloride solution (25 mL) and a 0.2 M aqueous  $\text{Na}_2\text{S}$  solution (25 mL) are prepared. Both precursor solutions are cooled to 0 °C in an ice bath and the synthesis is



performed at constant temperature (0 °C). While dropping the copper chloride solution to the sulfide solution under constant stirring, a dark-brown-black precipitation is observed. Subsequently, the suspension is centrifuged at 8000 rpm for 15 min and a powder is obtained, which is washed 5 times with Milli Q water without adjusting the pH value. The resulting product is dried under vacuum in a desiccator for 12 h at room temperature. The nanoparticles are characterized by XRD, TEM and Raman measurements.

**Sensor preparation:** Gas sensing measurements are done with commercial 3 mm x 3 mm alumina gas sensor substrates from UST-GmbH (Geschwenda/Germany). A platinum interdigital structure (IDS, gap width 25 µm) on top for electrical read out and a 10 Ω platinum built-in heater is integrated in these substrates. Small amounts of CuO particles are applied on the sensor substrate and fixed with one droplet of water.

**Sensing experiments:** The prepared sensors are mounted in a custom-made Teflon chamber (volume: 2 mL) and tested in a home-made gas sensing setup (similar to reference).<sup>[13]</sup> In this chamber defined gas mixtures containing H<sub>2</sub>S are supplied by mass flow controllers (MKS). Flow rates are adjusted to 120 sccm dry and 60 sccm humid synthetic air (PRAXAIR) with 20 sccm of diluted H<sub>2</sub>S in nitrogen (100 ppm) resulting in an atmosphere of 30 % relative humidity containing 10 ppm H<sub>2</sub>S.

For the electrical read-out a Keithley multimeter is used and the heater is controlled by a programmable laboratory power supply “K3005P” (by KORAD). Further characterization on the sensor substrates after sensing test is done by SEM and Raman measurements.

**Investigation of the regeneration of CuS:** For a detailed analysis of the regeneration during sensing experiments, commercial CuS is analysed by thermo gravimetric analysis (TG) on a STA 409PC thermoscale (Netzsch) in combination with a QMG421 quadrupole mass spectrometer (MS) by heating up the sample to 1000 °C with a heating rate of 5 °C/min. Additionally, the sample is heated up to 1000 °C in a furnace. At several temperature (160 °C, 200 °C, 300 °C, 350 °C, 450 °C, 550 °C, 850 °C, 1000 °C) a small amount of sample is removed from the furnace and characterized by XRD. For regeneration experiments in an atmosphere with a reduced amount of oxygen a home-made gas mixing setup is combined with a furnace. A curved glass tube is placed in a furnace and connected to a gas mixing setup based on four different mass flow controllers (see Supporting Information file, Figure S7). By decreasing the amount of synthetic air and increasing the amount of N<sub>2</sub> low oxygen concentrations are obtained. CuS is heated up to 450 °C in atmospheres containing a reduced partial pressure of O<sub>2</sub> (0.19 bar, 0.05 bar, 0.03 bar, 0.01 bar, 0.005 bar, 0 bar) in N<sub>2</sub> with 30 % relative humidity. The samples are characterized by XRD measurements.

## Acknowledgements

This project was supported by the Center for Materials Research of the Justus-Liebig-University Giessen, Germany. T. N. N. Lê, S. Gross and B. M. Smarsly acknowledge the double degree programme on Master's level in Chemistry/Materials Science between the Faculty of Biology and Chemistry of the Justus Liebig University, Giessen, Germany, and the Department of Chemical Sciences of the University of Padova, Italy. DAAD is acknowledged for a scholarship for T. N. N. Lê and supporting mutual visits. S. Gross thanks Dr. Nicola Dengo (University of Insubria, Italy) for his support in the optimization of the low

temperature synthesis of CuS nanostructures. Open Access funding enabled and organized by Projekt DEAL.

## Conflict of Interest

The authors declare no conflict of interest.

**Keywords:** copper oxide · copper sulfide · gas dosimeters · gas sensors · hydrogen sulfide

- [1] a) O. A. Habeeb, R. Kanthasamy, G. A. M. Ali, S. Sethupathi, R. B. M. Yunus, *Rev. Chem. Eng.* **2018**, *34*, 837-854; b) A. G. Georgiadis, N. D. Charisiou, M. A. Goula, *Catalysts* **2020**, *10*, 1-36.
- [2] a) R. J. Reiffenstein, W. C. Hulbert, S. H. Roth, *Annu. Rev. Pharmacol. Toxicol.* **1992**, *32*, 109-134; b) A. Aroca, C. Gotor, D. C. Bassham, L. C. Romero, *Antioxidants* **2020**, *9*, 1-23.
- [3] a) S. Pipatmanomai, S. Kaewluan, T. Vitidsant, *Appl. Energy* **2009**, *86*, 669-674; b) P. Fremerey, A. Jess, R. Moos, *J. Sensors Sens. Syst.* **2015**, *4*, 143-149; c) G. Korotcenkov, B. K. Cho, *Sens. Actuators B* **2011**, *156*, 527-538.
- [4] M. Elwood, *Int. J. Environ. Res. Public Health* **2021**, *18*, 1-17.
- [5] A. Paul, B. Schwind, C. Weinberger, M. Tiemann, T. Wagner, *Adv. Funct. Mater.* **2019**, *29*, 1904505.
- [6] a) Technical White Paper: Detecting Hydrogen Sulfide Gas and Understanding Its Danger in the Field. *Rosemount Anal. Inc.* **2015**; b) A. Mirzaei, S. S. Kim, H. W. Kim, *J. Hazard. Mater.* **2018**, *357*, 314-331.
- [7] a) A. Mirzaei, S. S. Kim, H. W. Kim, *J. Hazard. Mater.* **2018**, *357*, 314-331; b) J. Tamaki, T. Maekawa, N. Miura, N. Yamazoe, *Sens. Actuators B* **1992**, *9*, 197-203; c) A. Ponzoni, E. Comini, G. Sberveglieri, J. Zhou, S. Z. Deng, N. S. Xu, Y. Ding, Z. L. Wang, *Appl. Phys. Lett.* **2006**, *88*, 29-31; d) J. Kim, K. Yong, *J. Phys. Chem. C* **2011**, *115*, 7218-7224; e) D. D. Vuong, G. Sakai, K. Shimanoe, N. Yamazoe, *Sens. Actuators B* **2005**, *105*, 437-442; f) S. Steinhauer, *Chemosensors* **2021**, *9*, 1-20; g) S. Steinhauer, E. Brunet, T. Maier, G. C. Mutinati, A. Köck, O. Freudenberg, C. Gspan, W. Grogger, A. Neuhold, R. Resel, *Sens. Actuators B* **2013**, *187*, 50-57.
- [8] D. Li, Y. Tang, D. Ao, X. Xiang, S. Wang, X. Zu, *Int. J. Hydrogen Energy* **2019**, *44*, 3985-3992.
- [9] D. Li, X. Zu, D. Ao, Q. Tang, Y. Q. Fu, Y. Guo, K. Bilawal, M. B. Faheem, L. Li, S. Li, Y. Tang, *Sens. Actuators B* **2019**, *294*, 55-61.
- [10] a) N. Datta, N. S. Ramgir, S. Kumar, P. Veerender, M. Kaur, S. Kailasaganapathi, A. K. Debnath, D. K. Aswal, S. K. Gupta, *Sens. Actuators B* **2014**, *202*, 1270-1280; b) X. Liang, T. H. Kim, J. W. Yoon, C. H. Kwak, J. H. Lee, *Sens. Actuators B* **2015**, *209*, 934-942; c) A. Katoch, S. W. Choi, J. H. Kim, J. H. Lee, J. S. Lee, S. S. Kim, *Sens. Actuators B* **2015**, *214*, 111-116.
- [11] S. Steinhauer, *Chemosensors* **2021**, *9*, 1-20.
- [12] a) I. Marr, A. Groß, R. Moos, *J. Sensors Sens. Syst.* **2014**, *3*, 29-46; b) S. Steinhauer, E. Brunet, T. Maier, G. C. Mutinati, A. Köck, *Sens. Actuators B* **2013**, *186*, 550-556; c) K. Maier, A. Helwig, G. Müller, *Sens. Actuators B* **2017**, *244*, 701-708.
- [13] S. Werner, C. Seitz, G. Beck, J. Hennemann, B. M. Smarsly, *ACS Appl. Nano Mater.* **2021**, *4*, 5004-5013.
- [14] a) J. Hennemann, T. Sauerwald, C.-D. Kohl, T. Wagner, M. Bognitzki, A. Greiner, *Phys. Status Solidi A* **2012**, *209*, 911-916; b) C. Seitz, S. Werner, R. Marschall, B. M. Smarsly, *Zeitschrift für Phys. Chemie* **2018**, *233*, 105-116; c) J. Hennemann, C.-D. Kohl, B. M. Smarsly, H. Metelmann, M. Rohnke, J. Janek, D. Reppin, B. K. Meyer, S. Russ, T. Wagner, *Sens. Actuators B* **2015**, *217*, 41-50.
- [15] a) K. Maier, A. Helwig, G. Müller, *Sens. Actuators B* **2017**, *244*, 701-708; b) S. Werner, C. Seitz, G. Beck, J. Hennemann, B. M. Smarsly, *ACS Appl. Nano Mater.* **2021**, *4*, 5004-5013; c) J. Hennemann, T. Sauerwald, C.-D. Kohl, T. Wagner, M. Bognitzki, A. Greiner, *Phys. Status Solidi A* **2012**, *209*, 911-916; d) J. Hennemann, C.-D. Kohl, B. M. Smarsly, T. Sauerwald, J.-M. Teissier, S. Russ, T. Wagner, *Phys. Status Solidi A* **2015**, *212*, 1281-1288; e) J. Hennemann, C. D. Kohl, B. M. Smarsly, H. Metelmann, M. Rohnke, J. Janek, D. Reppin, B. K. Meyer, S. Russ, T. Wagner, *Sens. Actuators B* **2015**, *217*, 41-50; f) C. Seitz, S. Werner, R. Marschall, B. M. Smarsly, *Zeitschrift für Phys. Chemie* **2018**, *233*, 105-116; g) A. Paul, C. Weinberger, M. Tiemann, T. Wagner, *ACS Appl. Nano Mater.* **2019**, *2*, 3335.

- [16] C. Seitz, S. Werner, R. Marschall, B. M. Smarsly, *Zeitschrift für Phys. Chemie* **2018**, 233, 105-116.
- [17] a) A. Paul, B. Schwind, C. Weinberger, M. Tiemann, T. Wagner, *Adv. Funct. Mater.* **2019**, 29, 1904505; b) A. Paul, C. Weinberger, M. Tiemann, T. Wagner, *ACS Appl. Nano Mater.* **2019**, 2, 3335-3338.
- [18] Z. Yang, J. Xu, W. Zhang, A. Liu, S. Tang, *J. Solid State Chem.* **2007**, 180, 1390-1396.
- [19] a) A. Paul, B. Schwind, C. Weinberger, M. Tiemann, T. Wagner, *Adv. Funct. Mater.* **2019**, 29, 1904505; b) A. Paul, C. Weinberger, M. Tiemann, T. Wagner, *ACS Appl. Nano Mater.* **2019**, 2, 3335-3338; c) S. Werner, C. Seitz, G. Beck, J. Hennemann, B. M. Smarsly, *ACS Appl. Nano Mater.* **2021**, 4, 5004-58013; d) C. Seitz, S. Werner, R. Marschall, B. M. Smarsly, *Zeitschrift für Phys. Chemie* **2018**, 233, 105-116; e) J. Hennemann, C. D. Kohl, B. M. Smarsly, T. Sauerwald, J. M. Teissier, S. Russ, T. Wagner, *Phys. Status Solidi Appl. Mater. Sci.* **2015**, 212, 1281-1288.
- [20] a) M. Nafees, S. Ali, S. Idrees, K. Rashid, M. A. Shafique, *Appl. Nanosci.* **2013**, 3, 119-124; b) C. M. Simonescu, V. S. Teodorescu, O. Carp, L. Patron, C. Căpatina, *J. Therm. Anal. Calorim.* **2007**, 88, 71-76.
- [21] N. Dengo, A. Faresin, T. Carofiglio, M. Maggini, L. Wu, J. P. Hofmann, E. J. M. Hensen, P. Dolcet, S. Gross, *Chem. Commun.* **2020**, 56, 8707-8710.

---

Manuscript received: September 20, 2021  
Accepted manuscript online: November 3, 2021  
Version of record online: December 4, 2021